A Model for Fluid-Structure Interaction Problem with Inner Thin Shell Structures

Masahide KATAYAMA
Century Research Center Corp., Chiba, Japan
Tatsuhiko AIZAWA
University of Tokyo, Tokyo, Japan

ABSTRACT

An effective and efficient computational mechanics model is investigated to analyze a series of experimental tests simulating HCDA in LMFBR. The fluid-structure interaction with thin shell structures, especially containing the inner shell structures, is considered in the model. The calculational results are discussed by comparing reference experimental test data.

1 INTRODUCTION

In these two decades, various types of fluid-structure interaction analysis techniques have been proposed and investigated to consider severe accidents in the nuclear reactor facilities: e.g. Hypothetical Core Disruptive Accidents (HCDA) of the fast breeder reactors. Through those studies it has been verified that Eulerian/Lagrangian coupling technique in the Finite Difference Method (FDM) or Finite Element Method (FEM) is the most suitable and effective method to the fluid-structure interaction analysis. Authors have been concerned with this coupling technique to various problems, both in the nuclear and non-nuclear fields (Katayama et al. 1990 July, 1990 Oct.).

Since the full Lagrangian formulation is not adaptive to thin shell structures owing to the Courant condition, it is indispensable to imply thin shell solver to computer program and achieve Eulerian/shell coupling as well as Eulerian/Lagrangian coupling.

In the present paper, we will discuss over an appropriate model and some calculations by using a computer program for a series of experimental tests simulating HCDA. The fluid-structure interaction for the inner thin shell structures is taken into account of the proposing model. The calculated results are compared with the reference experimental data to demonstarate the effectiveness of our approach.

2 REFERENCE EXPERIMENTAL TESTS

A series of expeimental tests were carried out by PNC (Power Reactor and Nuclear Fuel Development Corporation) in order to ascertain the safety margin in the structural integrity of the reactor vessel and internal structures of the Japanese loop type LMFBR: proto-type Monju (Yoshie et al. 1987). In the tests the sodium coolant was replaced with water and the energy source of fuel/sodium interaction (FSI) was simulated by slow burning explosives. The parametric studies were performed to examine the following items: 1)scaling of vessel models, 2)energy release levels, 3)internal structures, 4)covergas gap levels and 5)material strength of vessel. That previous paper concluded that the final deformation profiles of reactor vessels can be classified into four typical patterns for various physical parameters in testing. Fig.1 lists these modes of deformations. The final deformation profiles of the reactor vessels in the experiments are shaped with such literal figures as 'B', 'D', 'b' and 'P'; in the followings these modes are cited as 'B'-, 'D'-, 'b'- and 'P'-modes.

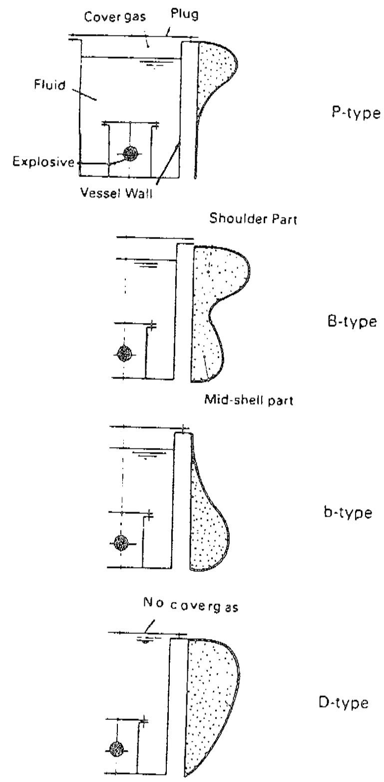

Fig.1 Final Deformation Patterns of Reactor Vessels (by Yoshie et al.)

3 CALCULATIONAL TECHNIQUE

The computational model is proposed and developed on the two dimensional explicit finite difference computer program: AUTODYN-2D. A Lagrange processor is used to model the solid continua and structures, a multiple material Euler processor for the fluids and the large distortion of solids, and a shell processor for thin structures. Mutual coupling of these processors enables us to deal with fluid-structure interaction problems (Birnbaum et al. 1987).

However, we come across a problem when applying the program to the HCDA analysis: consider the case when an Eulerian cell for fluid is divided into two regions by thin shell segments and thin shell interacts with fluid on both sides. It should be impossible to estimate their physical properties separately by usual or conventional treatment, as illustrated in Fig.2. The Eulerian cell can have only a single value for physical property: ϕ_A.

Then this problem will be solved by using the joined multiple Eulerian subgrid method, as shown in Fig.3.

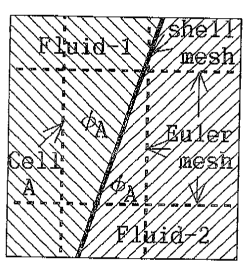

Fig.2 Euler cell: A to have only a single value for property: ϕ_A.

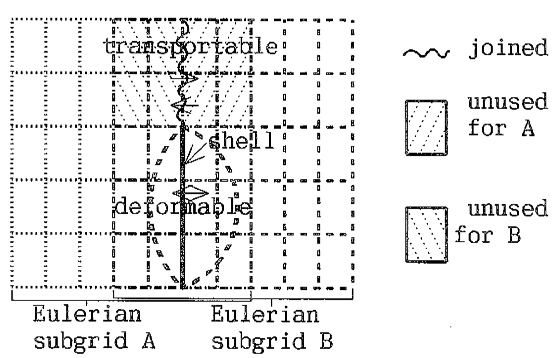

Fig.3 Joined Multiple Euler Subgrid Method

We use two Eulerian subgrids: A and B. They are joined with each other at the part of the waved line. Eulerian materials in a subgrid can advect to another subgrid through the seamed cell faces. The right-hand side of thin shell interacts with Eulerian materials in subgrid B, while its left-hand side with materials in subgrid A.

4 CALCULATION CONDITIONS

Three cases of calculations were performed. They are characterized in Table 1. Since the material strength of nickel becomes nearly the same as that of stainless steel in the elevated temperature region, some of tests were carried out by using the nickel vessels. We selected two different explosive charges: 20 g and 30 g, and two different depth covergases: 2.5 cm depth and no covergas.

The analytical geometry is shown in Fig.4. We selected 1/33 scale model in this study, while the reference experiments were performed against three different scale models. The reactor vessel is restrained at the upper end, but the lower end and core support can move freely.

The material models used in our calculations are shown in Table 2 except for the explosives. Since both stainless steel and nickel are subjected to the high strain rate loading, only dynamic stress-strain relations are employed as their constitutive equations. We used 'gasbag' model for the energy source. Through the experimental tests, P-δV relations were measured for the explosive and the air which existed initially in the core barrel (Yoshie, a private communication); P is the homogenized pressure and δV is the volume increment from the initial volume. Two different P-δV relations were used to investigate the effect of the explosive charges. In the calculational model the glass over the core barrel is neglected.

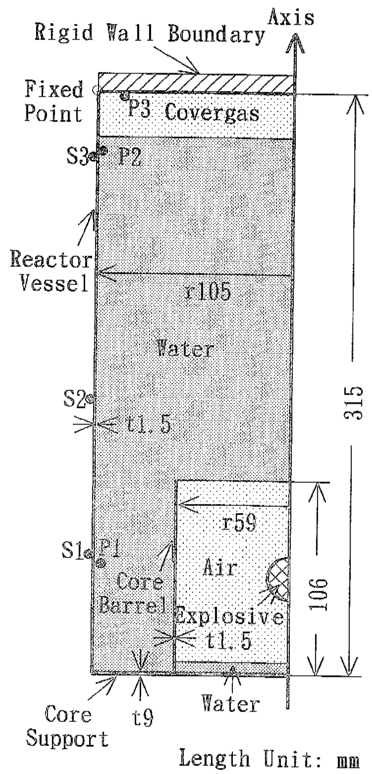

Fig.4 Calculatioal Geometry

Table 1 Calculational Parameters

Case No.	Vessel & Barrel	Explosive Charge	Covergas Depth	Pat-tern
1	Nickel	20 g	2.5 cm	B
2	SS304	20 g	0.0 cm	D
3	SS304	30 g	2.5 cm	P

5 RESULTS AND DISCUSSIONS

Fig.5 shows the velocity vector distributions at 2 msec for each case; figures are depicted with the same vector scaling. For both case-1 and case-3, with the covergas gaps in the initial stage, no covergas regions are

Table 2 Material Model Summary

Nickel	SS304
Density: 8.9 [g/cm^3]	Density: 7.8 [g/cm^3]
Bulk Modulus: 166.7 [GPa]	Bulk Modulus: 188.2 [GPa]
Shear Modulus: 76.92 [GPa]	Shear Modulus: 72.18 [GPa]
Strain [%] stress [GPa]	Strain [%] stress [GPa]
0.2 0.30	0.2 0.40
5.0 0.35	1.0 0.45
10.0 0.40	10.0 0.50
35.0 0.50	35.0 0.70

Water	Air
Density: 1.0 [g/cm^3]	Density: 1.225×10^{-3} [g/cm^3]
Hydro Tensile Limit: -3.0 [MPa]	Hydro Tensile Limit: 0.0 [MPa]
Equation of State:	Equation of State:
for compression regime ($\mu>0$)	$P=(\gamma-1)\rho e$,
$P=2.44\mu+3.41\mu^2+26.3\mu^3$ [GPa]	γ: 1.4 [-]
for tension regime ($\mu<0$)	where P is pressure, ρ is
$P=2.44\mu$ [GPa]	density and e is specific
where P is pressure and μ is	internal energy.
compression.	

observed, because they are compressed extremely. We can see large velocity vectors just below the shielding plug for both cases. This behavior might be caused by the covergases in multiple material Euler cells. The volume of gasbag region in case-1 becomes larger than the other cases. The related increase of velocities are also observed. These facts are explained by the effects of both compressibility of covergas and deformation of reactor vessel. The thin lines above the core barrel are also depicted to note the joined Euler seams in the analytical model.

The final hoop strain profiles of the reactor vessel for each case are shown in Fig.6. These results should be campared with the experimental results in Fig.7: these calculated hoop strain profiles are shaped in the same figures as observed in the

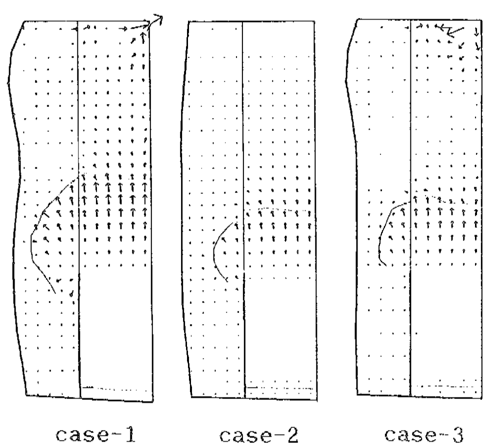

Fig.5 Velocity Vector Plots at 2 msec

experiments. About 20 % higher values of strain are obtained in the present analysis: this is because the homogenized P-δV relations, which are employed in computations, provides more stiff volumetric resistance. To be noted, only 5 % energy error is allowed in our explicit time integration as a tolerance, so that the time integration should affect the above behaviors.

Fig.8 indicates the total strain histories at the selected points shown in Fig.4 for case-1; the solid line shows the hoop strain and the dotted line the meridional. Those predicted strain histories are also in good agreement with the experimental results shown in Fig.9. These two results are apparently different from the strain histories for the case-2 in Fig.10. Let us consider this difference by citing the pressure histories at typical three points of P1, P2 and P3 in Fig.11 and 12 for two cases. A sharp peak pressure appears at P3 about 1.2 msec in Fig.11. This high pressure is caused by the compression of covergas, and after that lower peaks appear at P2 a little bit lower than P3. The pressure histories for both cases at P1 in the vicinity of the core barrel are bounded by the lower level and almost just the same for two cases. From about 1 msec covergas starts to be compressed, as the gasbag region expands. At the moment the covergas is compressed extremely, the slug impact of the water occurs against the rigid wall boundary. Then the flow of the water turns to the radial direction and cause the deformation of shoulder part of the reactor vessel.

6 CONCLUSIONS

Through the present study, we have constructed the effective and efficient computational model of the fluid-structure interaction with the inner thin structure to

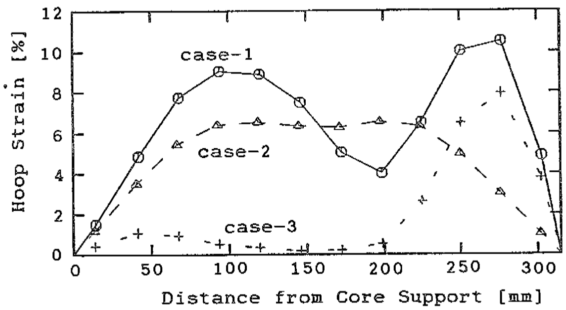

Fig.6 Final Hoop Strain Distribuion in the Ractor Vessel (Calculation)

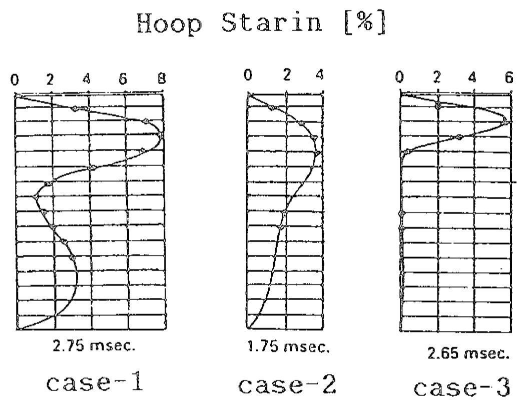

Fig.7 Final Hoop Strain Profiles in the Ractor Vessel (Experiment)

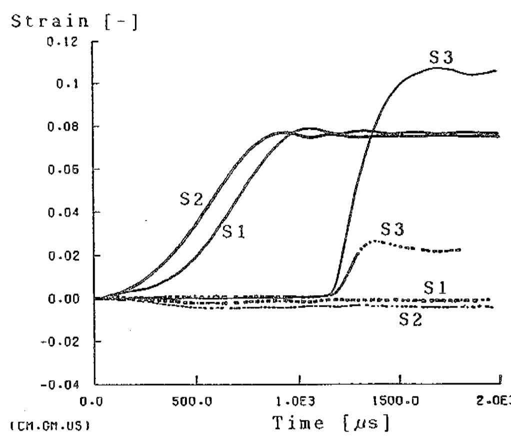

Fig.8 Total Strain Histories for case-1 (Calculation)

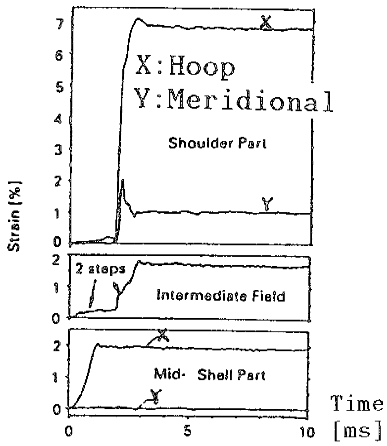

Fig.9 Total Strain Histories for case-1 (Experiment)

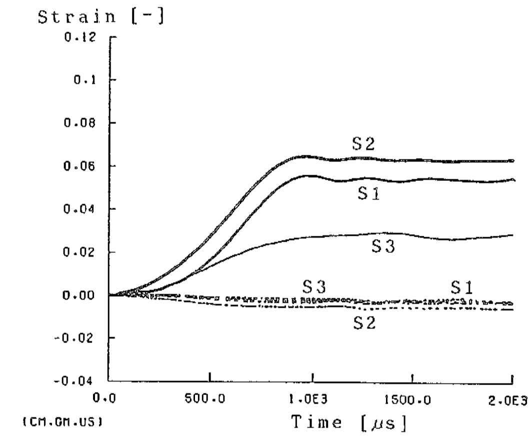

Fig.10 Total Strain Histories for case-2 (Calculation)

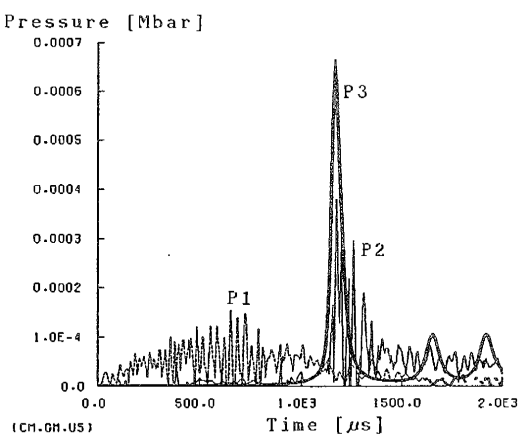

Fig.11 Pressure Histories for case-1 (Calculation)

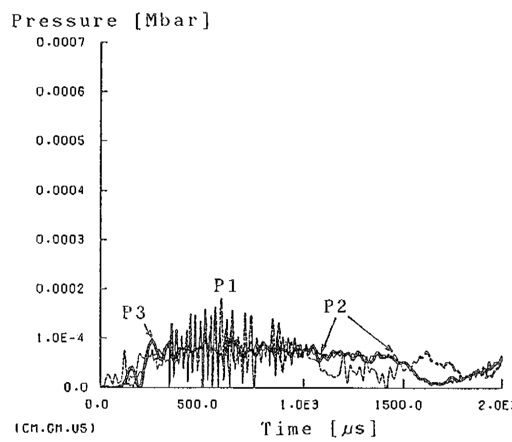

Fig.12 Pressure Histories for case-2 (Calculation)

deal with HCDA of LMFBR. The calculated results by the computer program are in fairly good agreement with those of the reference experimental tests. Through these physical modeling and simulations, we can comprehend the physical phenomena of HCDA in LMFBR.

REFERENCES

Katayama,M. and Aizawa,T. (1990 July).A Visualized Analysis of Fluid Structure Interaction Problem, Proc. of Symp. on Comp. Methods in Struct. Eng. and Related Fields, Vol.14, pp.173-178, (in Japanese)

Katayama,M.,Aizawa, T. and Tanaka,K. (1990 Oct.).Analysis of Shock Wave Structure in the Free Surface Water of Explosive Free Forming Assembly, The Proc. of the 41st Jap. Joint Conf. for the Tech. of Plasticity, pp.183-186

Yoshie,S. and Saito,M. (1987). Shock structural response of reactor vessel under HCDA in LMFBR, SMiRT-9, Vol.E, pp.325-330

Birnbaum,N.K. et al. (1987). AUTODYN - an interactive non-linear dynamic analysis program for microcomputers through supercomputers, SMiRT-9, Vol.B, pp.401-405